ChemComm

COMMUNICATION

View Article Online
View Journal | View Issue

Cite this: *Chem. Commun.*, 2023, 59, 10761

Received 4th July 2023,
Accepted 31st July 2023

DOI: 10.1039/d3cc03208f

rsc.li/chemcomm

Effects of intermetal distance on the electrochemistry-induced surface coverage of M–N–C dual-atom catalysts†

Weijie Yang, *[a] Zhenhe Jia,[a] Liugang Chen,[a] Binghui Zhou,[a] Di Zhang,[b] Yulan Han,[c] Zhengyang Gao[a] and Hao Li *[b]

The often-overlooked electrocatalytic bridge-site poisoning of the emerging dual-atom catalysts (DACs) has aroused broad concerns very recently. Herein, based on surface Pourbaix analysis, we identified a significant change in the electrochemistry-induced surface coverages of DACs upon changing the intermetal distance. We found a pronounced effect of the intermetal distance on the electrochemical potential window and the type of pre-covered adsorbate, suggesting an interesting avenue to tune the electrocatalytic function of DACs.

Understanding the surface coverages of an electrocatalyst under electrochemical conditions is crucial because the potential-dependent surface coverages determine properties of the initial reaction surface.[1] Owing to the occurrence of electrochemical reactions at the electrolyte-electrode interface, cations or anions from hydrolysis have the potential to occupy the catalytic sites, leading to a substantial deterioration in the catalytic performance.[2,3] Unfortunately, precise *in situ* methods for probing the actual surface are still limited, posing a significant challenge for experimental investigations.

To gain a profound understanding of electrochemistry-induced surface coverages, surface Pourbaix analysis is used to provide a theoretical framework for investigating the most electrochemically favourable structure within distinct reaction contexts.[4,5] Hansen *et al.*[6] observed that alterations in the electrolyte pH and applied potentials induce modifications in surface coverages of some metal catalysts (*e.g.*, Pt, Ag, and Ni). Dobrota *et al.*[7] developed surface Pourbaix diagrams for some single-atom catalysts (SACs), revealing that the presence of H*, O*, and HO* species under certain reaction potentials could impede the accessibility of active sites. As examples of atomic dispersion catalysts, dual-atom catalysts (DACs) have been anticipated to exhibit multifunctionality or enable profound electrochemistry due to their containing multi-metal sites.[8–10] In our previous work, we conducted an analysis of the electrochemistry-induced surface coverages of various Fe/Ni DACs with different N/C coordination environments. Our findings indicated an effect of the number of coordinating N atoms on surface coverages.[11] Subsequently, Zhang *et al.*[12] used surface Pourbaix analysis to identify N_3–Co–Ni–N_2 as a promising electrocatalyst for nitrogen reduction. However, relating the identification of factors influencing surface coverages with the development of effective strategies for tuning catalytic structures remains a significant challenge.

Previous research has indicated that tuning the solution conditions (*e.g.*, pH and applied potential) could tackle the electrochemistry-induced surface coverage effectively. Additionally, modulating the structure of the catalyst represents another viable approach to achieving desired surface characteristics. Jiao *et al.*[13] observed that engineering the microenvironment around catalytic sites can improve the performance of MOF-based catalysts by adjusting the geometry and spatial distribution. Ha *et al.*[14] screened SACs with 3d–5d transition metals for oxygen electrocatalysis by investigating their coordination environments. Very recently, Yao *et al.*[15] showed 5.3 Å to be the threshold distance of Ni/Cu-N-C, which exhibited a synergistic promotion of the adsorption of intermediates, thus boosting the activity and selectivity of CO_2 reduction. However, further investigation is still needed to understand the influence of atomic-scale effects on the electrochemistry-induced surface coverages of DACs.

Motivated by the current research progress, herein we developed five distinct configurations of DAC and DAC-like materials with different intermetal distances (*i.e.*, metal–metal distance in bimetallic systems). Considering the distinction between homo- and heteronuclear DACs, Fe/Co and Fe/Fe were selected as the metal centres due to the extensive experimental and theoretical investigations on them.[16,17] Utilizing spin-polarized

[a] *Department of Power Engineering, School of Energy, Power and Mechanical Engineering, North China Electric Power University, Baoding 071003, China. E-mail: yangwj@ncepu.edu.cn*
[b] *Advanced Institute for Materials Research (WPI–AIMR), Tohoku University, Sendai 980–8577, Japan. E-mail: li.hao.b8@tohoku.ac.jp*
[c] *School of Chemistry and Chemical Engineering, Queen's University Belfast, Belfast BT9 5AG, UK*

† Electronic supplementary information (ESI) available. See DOI: https://doi.org/10.1039/d3cc03208f

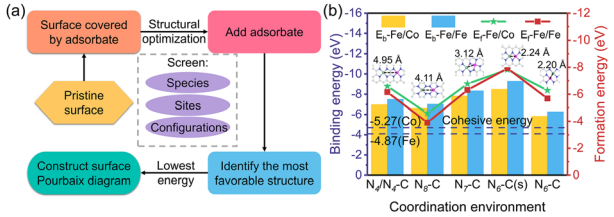

Fig. 1 Process of developing a surface Pourbaix diagram and stability analysis of DAC and DAC-like materials. (a) Flowchart of the development of a surface Pourbaix diagram for surface coverage analysis. Starting from the pristine surface of a DAC, the adsorption Gibbs free energies of various adsorbates were obtained from DFT calculations. Afterward, the lowest energy one was selected for surface Pourbaix diagram construction. (b) Stability analysis of ten DAC and DAC-like materials.

density functional theory (DFT) calculations, we derived 1D and 2D surface Pourbaix diagrams by considering the Gibbs adsorption free energies of H*, O*, and HO* on DACs. These diagrams revealed that some undesirable adsorbates from solvents can be adsorbed onto the surface within a specific potential range. (A flowchart of how to develop a surface Pourbaix diagram for surface coverage analysis is shown in Fig. 1a.) Furthermore, we evaluated the impact of metal type, number of coordinated N atoms, and intermetal distance on the electrochemical potential window (EPW),[11] which describes the range of potentials of the pristine state. This work has presented a catalyst design strategy involving modifying electrochemistry-induced surface coverages by manipulating intermetal distance, thereby providing a targeted approach for optimizing catalytic performance.

In this study, all DFT calculations were performed utilizing the Vienna *ab initio* simulation package (VASP) with the Perdew–Burke–Ernzerhof (PBE) functional and projector-augmented wave (PAW) potentials.[18–24] More details about the computations can be found in the Computational Methods section and Tables S1–S2 of ESI.†

Stability should be the highest-priority characteristic to be considered in catalyst design.[25,26] In this work, five different configurations of DACs, with different intermetal distances, were constructed. The selected metal centres were Fe/Co and Fe/Fe, with a coordination environment of pyridine N dopants in graphene.[27] According to the intermetal distance and the number of coordinating N atoms, the DACs were named Fe–N_4/Co (Fe)–N_4–C, Fe/Co (Fe)–N_8–C, Fe/Co (Fe)–N_7–C, Fe/Co (Fe)–N_6–C (s), and Fe/Co (Fe)–N_6–C, respectively (Fig. 1b and Fig. S1, ESI†). Binding energy (E_b), formation energy (E_f), and cohesive energy (E_{coh}) values were calculated to evaluate the stability of these DACs (Fig. 1b). All these values exhibited a negative sign, indicating good thermodynamic stability. Furthermore, the E_b value was calculated to be more negative than E_{coh}, suggesting a favourable avoidance of metal centre aggregation. Note that similar values of E_b and E_{coh} were found on Fe/Co–N_6–C; to further assess the structural stability, simulations of *ab initio* molecular dynamics (AIMD)[28] were employed at 300 K for 12 ps (Fig. S2, ESI†). The energies and average bond lengths exhibited oscillations within a narrow range, providing evidence of high stability.

To analyse the electrochemistry-induced surface coverages under aqueous conditions, multiple adsorption configurations of H*, O* and HO* were calculated (Fig. S3–S12, ESI†). These configurations indicated a critical role played by the intermetal distance in determining the presence or absence of the metal bridge site. A decreasing intermetal distance was indicated to be associated with an increasing synergistic effect between the metals, leading to a preference for adsorption at the bridge site. Moreover, we observed the adsorption of H*, O*, and HO* occurring at the metal-atop site until the intermetal distance was decreased to approximately 2.24 Å. In the cases of Fe/Fe–N_6–C (s), Fe/Co–N_6–C, and Fe/Fe–N_6–C, the small intermetal distance was indicated to generate strong synergistic effects, leading to adsorption at the bridge site. However, for other DACs with a metal–metal distance greater than 2.24 Å, the adsorption was indicated to predominantly occur at the metal-atop site. To better understand the site effect, we have denoted the adsorbates at different adsorption sites using subscript labels (*e.g.*, with $1H_{Bri}1H_{Fe\text{-}atop}$ representing one H adsorbed at the bridge site and another H adsorbed at the Fe-atop site).

Based on the thermodynamically favourable coverages, we developed surface Pourbaix diagrams for ten DACs at pH = 0, as shown in Fig. 2. Inspection of these Pourbaix diagrams showed a significant influence of the applied potential (U_{RHE}) on the adsorption states for constant pH—with H-containing molecules (*e.g.*, H* and 2H*) more readily adsorbed onto the surface at negative potentials, but O-containing molecules (*e.g.*, O*, 2O*, HO*, and 2HO*) favouring the occupying of the active sites at positive potentials. In particular, we observed the surface of Fe/Co (Fe)–N_6–C remaining consistently occupied throughout the entire range of potentials (Fig. 2i–j), but with other configurations exhibiting pristine surfaces at certain potential ranges (Fig. 2a–h). Additionally, adjusting the metal type within the same configuration also led to a change in the electrochemistry-induced surface coverages (*e.g.*, homo- and heteronuclear DACs in Fig. 1a and 1b). However, this effect for late 3d metals (*e.g.*, Fe and Co) was found to be relatively minor compared to the impact of modifying the intermetal distance.

Given the multifunctionality of DACs, which in general allows catalysts to be used for various reactions, it was important to consider that the conditions of the solution may have an impact on the surface coverages induced by electrochemistry. Therefore, we set out to analyse the surface coverages of DACs comprehensively; and to do so, we further developed the surface Pourbaix diagrams of these models as a function of potential and pH (Fig. S13, ESI†). The diagrams were partitioned into multiple regions exhibiting distinct surface coverages, each representing the distinct surface coverages that would respond to changes in potential and pH. All regions were observed to exhibit an apparent linear variation in response to change in pH. Furthermore, as the intermetal distance was varied, the partitioning of regions also changed, indicating a modification in the electrochemistry-induced surface coverage of the DAC. Notably, in the case of Fe/Co (Fe)–N_6–C (Fig. S11i–j, ESI†), as the potential was made more positive, 1O* and 1HO* preferentially

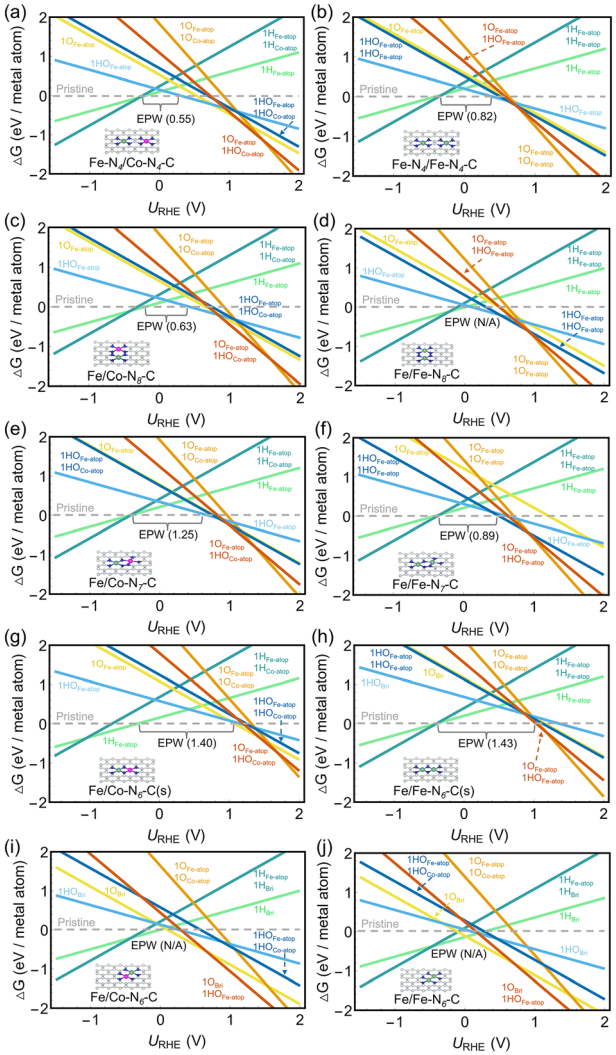

Fig. 2 Electrochemistry-induced surface coverages of DAC and DAC-like materials. (a–j) Surface Pourbaix diagrams of (a) Fe–N_4/Co–N_4–C, (b) Fe–N_4/Fe–N_4–C, (c) Fe/Co–N_8–C, (d) Fe/Fe–N_8–C, (e) Fe/Co–N_7–C, (f) Fe/Fe–N_7–C, (g) Fe/Co–N_6–C (s), (h) Fe/Fe–N_6–C (s), (i) Fe/Co–N_6–C, and (j) Fe/Fe–N_6–C.

occupied the metal centre instead of 2O* (Fig. S11a–h, ESI†), which can be attributed to adsorption at the bridge site. The absence of any single atom bridging the two metals would provide a better chance to stabilize the oxo-bridged bimetallic core. As a result of the different adsorption tendencies of O* and HO*, O* exhibited stronger adsorption on the bridge site, whereas HO* showed stronger adsorption on the atop site. The 2D surface Pourbaix analysis further confirmed the substantial influence of the intermetal distance on the surface coverages.

Considering the diversity of electrochemical reactions, we analyzed various reactions at five typical operating potentials, specifically the oxygen evolution reaction (OER) at 1.60 V_{RHE}, oxygen reduction reaction (ORR) at 0.78 V_{RHE}, hydrogen evolution reaction (HER) at 0 V_{RHE}, CO_2 reduction reaction (CO_2RR) at −0.35 V_{RHE}, and nitrogen reduction reaction (NRR) at −0.4 V_{RHE}, to investigate the electrochemistry-induced surface

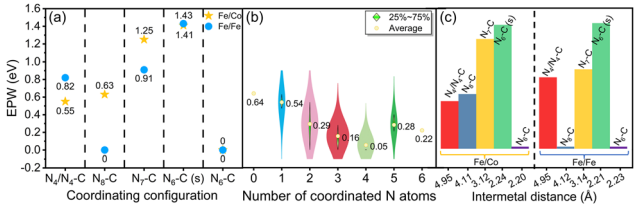

Fig. 3 Variations of the electrochemical potential windows (EPWs) of the DAC and DAC-like materials analyzed in this study: variations associated with changing (a) metal type, (b) number of coordinating N atoms (with the values referring to ref. 11), and (c) intermetal distance.

coverages (Fig. S14, ESI†).[11] Under ORR conditions, the occupation of most Fe/Ni–N_x–C structures can change from O* to HO* with the increase of the intermetal distance. Similarly, under the CO_2RR operating potential, the change in coverage caused by tailoring intermetal distance was more significant than by adjusting the number of coordinating N atoms. Based on these findings, we developed a catalytic design strategy that focused on tailoring the intermetal distances to regulate the electrochemistry-induced surface coverages of DACs, thereby obtaining a regulation of the reaction process.

To comprehensively examine the influence of the intrinsic structural factors on the electrochemistry-induced surface coverages of DACs, we analysed the distribution of the EPW of our models (Fig. 3). In experiments, the strategies to regulate the type of DACs mainly involve controlling the metal type, intermetal distance, and coordination environment of the metal atoms. Therefore, we focused on analysing the impact of metal type, number of coordinating N atoms, and intermetal distance on EPW. We observed a slight fluctuation in the EPW when changing the type of metal (Fig. 3a). Similarly, altering the number of coordinating N atoms while keeping the same configuration was also observed to affect the value of EPW. As shown in Fig. 3b, by tailoring the number of coordinating N atoms for a series of typical Fe/Ni–N_x–C species, we observed fluctuations within a moderate range. Most importantly, tailoring the intermetal distance can result in a significant change in the EPW by altering the adsorption sites, unlike the effects of changing the metal type and number of coordinating N atoms, which would only modify the angle between adsorbates and DACs in the adsorption structure (Fig. 3c). These findings highlighted the crucial role of the intermetal distance in determining the electrochemical surface coverages of late-3d-metal-based DACs, which may surpass the influence of metal type and the number of coordinating N atoms.

To further analyse the potential relationship between the electrochemistry-induced surface coverages and intermetal distance, we developed linear correlations between system electronegativity or the adsorption energy of O*/HO* *vs.* intermetal distance (Fig. 4a–c). The intermetal distance was concluded from these plots to affect both the system electronegativity and the adsorption behaviour of O*/HO*, thereby influencing the surface coverage of DACs. As the intermetal distance was decreased, the system electronegativity also decreased, leading to weaker adsorption of O*/HO*. However, when the intermetal

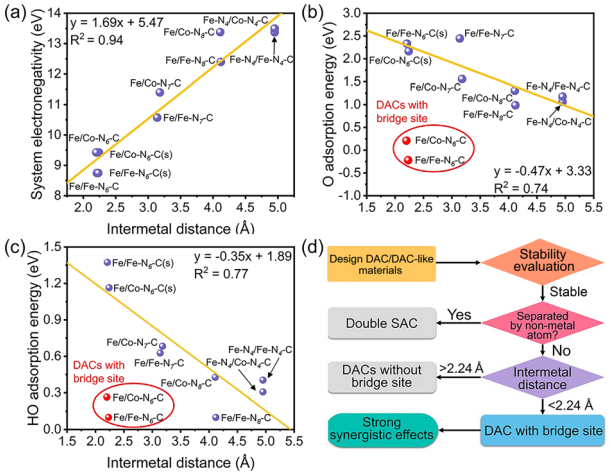

Fig. 4 Observation of linear relationships with intermetal distance and the process used to identify the types of DAC and DAC-like materials. (a) Plot of system electronegativity *vs.* intermetal distance. (b) Plot of O* adsorption energy *vs.* intermetal distance. (c) Plot of HO* adsorption energy *vs.* intermetal distance. (d) Flowchart for identifying the types of DAC and DAC-like materials.

distance was set at less than about 2.24 Å, the occurrence of bridge site adsorption behaviour enhanced the O*/HO* adsorption strength, leading to a significant alteration in the electrochemistry-induced surface coverages. Based on the above results, a flowchart was developed to illustrate the identification of DAC and DAC-like materials using interatomic distance as the key independent variable (Fig. 4d). In the case of non-metal atoms (*e.g.*, C or N) present between the two metals, the catalysts would more likely be classified as double SACs. Otherwise, the intermetal distance was used to categorize the types of DACs. Taking Fe-series DACs as an example, metal–metal atoms with a threshold distance of less than 2.24 Å were found to exhibit bridge-site adsorption behaviour and a strong synergistic effect regulating the electronic structure and promoting adsorption, ultimately determining the electrochemistry-induced surface coverage.

In summary, this work revealed that different DAC structures exhibit distinct electrochemically induced surface coverages, leading to the presence of various active sites and electronic structures. Importantly, our findings for late 3d metals (*e.g.*, Fe and Co) highlighted that, compared to metal type and number of coordinating N atoms, intermetal distance may play a more prominent role in determining the electrochemistry-induced surface coverage of DACs. By plotting O*/HO* adsorption energy *versus* intermetal distance and drawing straight lines through the plots, we uncovered the underlying mechanism by which the intermetal distance influences the system electronegativity and the adsorption characteristics of O*/HO* on metal or bridge sites, ultimately affecting the surface coverage. Further analysis of the mechanism related to intermetal distance will be explored in our future research. Additionally, we provided a flowchart that utilizes interatomic distance as the key independent variable to elucidate the identification of DAC and DAC-like materials. This research has led to a catalyst design strategy involving modifying the electrochemistry-induced surface coverages by manipulating intermetal distance, thereby providing an interesting new avenue for optimizing catalytic performance. We hope that our future work will provide a more comprehensive and insightful understanding of the family of DAC catalysts.

This work was supported by the National Natural Science Foundation of China (No. 52006073 and 52176104), the Fundamental Research Fund for the Central Universities (2023MS125), JSPS KAKENHI (No. JP23K13703), and Iwatani Naoji Foundation.

Conflicts of interest

There are no conflicts to declare.

References

1 H. Li, *et al.*, *J. Phys. Chem. Lett.*, 2022, **13**, 2057–2063.
2 L. Zhou, *et al.*, *ACS Energy Lett.*, 2022, **7**, 993–1000.
3 H. Li, *et al.*, *Nat. Catal.*, 2021, **4**, 463–468.
4 O. Vinogradova, D. Krishnamurthy, V. Pande and V. Viswanathan, *Langmuir*, 2018, **34**, 12259–12269.
5 S. Pan, *et al.*, *Nat. Commun.*, 2022, **13**, 2294.
6 H. A. Hansen, J. Rossmeisl and J. K. Nørskov, *Phys. Chem. Chem. Phys.*, 2008, **10**, 3722–3730.
7 A. S. Dobrota, N. V. Skorodumova, S. V. Mentus and I. A. Pašti, *Electrochim. Acta*, 2022, **412**, 140155.
8 Y. Yang, *et al.*, *Sci. Adv.*, 2020, **6**, eaba6586.
9 J. Zhang, *et al.*, *Chin. J. Catal.*, 2020, **41**, 783–798.
10 R. Li and D. Wang, *Adv. Energy Mater.*, 2022, **12**, 2103564.
11 W. Yang, *et al.*, *Commun. Chem.*, 2023, **6**, 6.
12 Y. Zhang, *et al.*, *J. Colloid. Interfaces Sci.*, 2023, **640**, 983–989.
13 L. Jiao, J. Wang and H. Jiang, *Acc. Mater. Res.*, 2021, **2**, 327–339.
14 M. Ha, *et al.*, *Energy Environ. Sci.*, 2021, **14**, 3455–3468.
15 D. Yao, *et al.*, *Adv. Mater.*, 2023, **35**, 2209386.
16 S. Cao, *et al.*, *Energy Environ. Mater.*, 2023, **6**, e12287.
17 Y. Yan, *et al.*, *J. Mater. Chem. A*, 2021, **9**, 19489–19507.
18 J. Hafner, *J. Comput. Chem.*, 2008, **29**, 2044–2078.
19 I. C. Lin, A. P. Seitsonen, I. Tavernelli and U. Rothlisberger, *J. Chem. Theory Comput.*, 2012, **8**, 3902–3910.
20 G. Kresse and D. Joubert, *Phys. Rev. B: Condens. Matter Mater. Phys.*, 1999, **59**, 1758.
21 A. V. Krasheninnikov, P. O. Lehtinen and A. S. Foster, *Phys. Rev. Lett.*, 2009, **102**, 126807.
22 J. Klimeš and A. Michaelides, *J. Chem. Phys.*, 2012, **137**, 120901.
23 W. Yang, *et al.*, *J. Hazard. Mater.*, 2022, **421**, 126639.
24 W. Yang, *et al.*, *Electrochim. Acta*, 2020, **335**, 135667.
25 Q. Zhou, M. Zhang, B. Zhu and Y. Gao, *Nanomaterials*, 2022, **12**, 2557.
26 Y. Qian, *et al.*, *EcoMat*, 2020, **2**, e12014.
27 C. Chen, *et al.*, *Energy Environ. Sci.*, 2023, **16**, 1685–1696.
28 M. E. Tuckerman, P. J. Ungar, T. Von Rosenvinge and M. L. Klein, *J. Phys. Chem.*, 1996, **100**, 12878–12887.